QUARTERLY JOURNAL OF THE ROYAL METEOROLOGICAL SOCIETY
Q. J. R. Meteorol. Soc. **135**: 1643–1660 (2009)
Published online 1 October 2009 in Wiley InterScience
(www.interscience.wiley.com) DOI: 10.1002/qj.498

Meridional energy transport in the coupled atmosphere–ocean system: Scaling and numerical experiments

Geoffrey K. Vallis* and Riccardo Farneti
GFDL, Princeton University, USA

ABSTRACT: We explore meridional energy transfer in the coupled atmosphere–ocean system, with a focus on the extratropics. We present various elementary scaling arguments for the partitioning of the energy transfer between atmosphere and ocean, and illustrate those arguments by numerical experimentation. The numerical experiments are designed to explore the effects of changing various properties of the ocean (its size, geometry and diapycnal diffusivity), the atmosphere (its water vapour content) and the forcing of the system (the distribution of incoming solar radiation and the rotation rate of the planet). We find that the energy transport associated with wind-driven ocean gyres is closely coupled to the energy transport of the midlatitude atmosphere so that, for example, the heat transport of both systems scales in approximately the same way with the meridional temperature gradient in midlatitudes. On the other hand, the deep circulation of the ocean is not tightly coupled with the atmosphere and its energy transport varies in a different fashion.

Although for present-day conditions the atmosphere transports more energy polewards than does the ocean, we find that a wider or more diffusive ocean is able to transport more energy than the atmosphere. The polewards energy transport of the ocean is smaller in the Southern Hemisphere than in the Northern Hemisphere; this arises because of the effects of a circumpolar channel on the deep overturning circulation. The atmosphere is able to compensate for changes in oceanic heat transport due to changes in diapycnal diffusivity or geometry, but we find that the compensation is not perfect. We also find that the transports of both atmosphere and ocean decrease if the planetary rotation rate increases substantially, indicating that there is no a priori constraint on the total meridional heat transport in the coupled system. Copyright © 2009 Royal Meteorological Society

KEY WORDS climate dynamics; coupled atmosphere–ocean models; climate theory

Received 14 October 2008; Revised 9 July 2009; Accepted 21 July 2009

1. Introduction

The meridional energy transport in the atmosphere and ocean is one of the most fundamental aspects of the climate system, for it largely determines how the weather and climate vary with latitude. The advent of satellite measurements of the top-of-the-atmosphere radiative balance coupled with reanalyses of the surface energy fluxes and/or atmospheric circulation have led to quantitative estimates of the the total energy transfer (via the radiative balance), atmospheric energy transfer (via the surface fluxes and reanalyses) and therefore the implied oceanic energy transfer (Trenberth and Caron, 2001). Direct estimates of the oceanic transfer are quite difficult because of the relative lack of oceanic observations, especially in the abyss, but such estimates are slowly becoming available (Ganachaud and Wunsch, 2000). The overall picture is that at very low latitudes the polewards energy transport in the ocean exceeds that of the atmosphere, but in midlatitudes the atmospheric transport is two or three times that of the ocean. Coupled general circulation models (GCMs) of the modern era are generally able to simulate this transport reasonably well, but our understanding of the transport, especially in the coupled system, has kept pace with neither observations nor simulations. We do not properly understand why the transport has the form it does, how that transport might change if the geometry or physical parameters of the system were to change, and whether the form of the transport reflects some more fundamental aspects of the climate system other than the particular combination of physical parameters and geography existing on the present-day Earth. These questions are the subject of this article.

It seems unlikely that we can make headway on these issues via a purely analytic approach without numerical models. Thus in this article we describe the use of a combination of a simply configured coupled atmosphere–ocean model with a variety of scaling arguments to try to make estimates of the magnitude, distribution and partitioning of the energy transport in the atmosphere and ocean. We are concerned with understanding how general the transport is, and how it might change with different parameters in the system – the rotation of the Earth, the diapycnal diffusivity of the ocean, the presence of moisture in the atmosphere, and so forth. Suppose that the parameters and hence the energy transport

*Correspondence to: Geoffrey K. Vallis, GFDL, Princeton University, USA. E-mail: gkv@princeton.edu

of one subsystem (i.e. atmosphere or ocean) change, or that the energy transport of one subsystem changes temporally because of natural variability. Will the transport in the other subsystem then compensate for or reinforce those initial changes?

Previous theoretical work has predominantly focused on oceanic transport or atmospheric transport individually. Thus, for example, Bye and Veronis (1980) and Wang *et al.* (1995) studied heat transport in ocean gyres, and Barry *et al.* (2002), Caballero and Langen (2005), Schneider and Walker (2008) and Zurita-Gotor and Vallis (2009) explored heat transport in the atmosphere as various parameters vary. In this article our goal is to better understand the coupled system, focusing on midlatitude dynamics; there is less previous work on the coupled problem, but we note that Held (2001) looked at the partitioning of energy transport between the atmosphere and ocean in the Tropics and Enderton and Marshall (2009) recently presented some coupled simulations of a similar nature to ours. Our general approach is to mechanistically divide the atmosphere and ocean into various components and then to use the simplest possible arguments to derive estimates for the energy transport in these components or, where this is not possible, for the partitioning of the energy transport between components such as the midlatitude atmosphere and wind-driven gyres. We then test our theoretical predictions using a numerical coupled ocean–atmosphere model. The model has an idealized geometry and simplified physical parametrizations, allowing a broader range of parameters to be varied and much longer integrations to be carried out than would be possible with a full GCM. The parameters we vary include the oceanic diapycnal diffusivity, the width and depth of the ocean, the amount of water vapour in the atmosphere, the Earth's rotation rate and the distribution of solar insolation at the top of the atmosphere.

We have chosen to present the scaling arguments – much of which comprise review material – prior to the numerical experiments, in sections 2–5. However, the reader may prefer to go directly to the numerical experiments in sections 6–11, referring back as needed, and we have tried to write the article so that this is possible.

2. Basic formulae

In both the atmosphere and ocean the kinetic energy is a small contributor to the total meridional energy transfer; the remaining transfer may be referred to as the static energy transfer or, with an abuse of terminology, the 'heat' transfer, and for a dry atmosphere it is equal to the transfer of enthalpy. The Earth's atmosphere is very nearly an ideal gas, so that the energy or heat transfer is then given by

$$\begin{aligned} E_\mathrm{a} &= \int \rho v \left(I + gz + Lq + \frac{p}{\rho} \right) \mathrm{d}x\mathrm{d}z \\ &= \int (S_\mathrm{d} + Lq) v\rho \mathrm{d}x\mathrm{d}z = \int S_\mathrm{m} v \rho \mathrm{d}x\mathrm{d}z, \end{aligned} \tag{2.1}$$

where the integral is taken over the depth of the fluid and around a latitude circle, v is the meridional velocity, $I = c_v T$ is the internal energy, L is the latent heat of condensation, q is the specific humidity, $S_\mathrm{d} = c_p T + gz$ is the dry static energy and $S_\mathrm{M} = S_\mathrm{d} + Lq$ is the moist static energy. The 'gross stability' of the atmosphere, S_a, may be defined as the ratio of energy transfer to mass transfer (Neelin and Held, 1987), and a corresponding 'gross temperature', $\hat{\theta}_\mathrm{a}$, may be defined by $\hat{\theta}_\mathrm{a} = S_\mathrm{a}/c_p$.

To a good approximation the meridional energy transport in the ocean is given by (Warren, 1999)

$$E_\mathrm{o} = \int c_\mathrm{o} \rho_o v \theta \mathrm{d}x\mathrm{d}z, \tag{2.2}$$

where θ is the potential temperature, c_o is the heat capacity of seawater per unit mass at the top of the ocean and ρ_o is the reference density used in the Boussinesq approximation. The gross stability of the ocean, S_o, may similarly be defined as the ratio of energy transfer to mass transfer, and a corresponding gross temperature may be defined as $\hat{\theta}_\mathrm{o} = S_\mathrm{o}/c_\mathrm{o}$.

It is useful to express the energy transports as integrals of an appropriate stream function over an energy coordinate. This is a common procedure in ocean modelling (Bryan and Sarmiento, 1985) and the oceanic energy transport E_o is then given by

$$E_\mathrm{o}(y) = c_\mathrm{o} \int V \theta \mathrm{d}\theta, \tag{2.3}$$

where the integral is over the full range of potential temperature present. The quantity V is the mass transport per unit temperature interval, similar to a thickness-weighted meridional velocity. It may be expressed in terms of a stream function Ψ_o such that $V = -\partial \Psi_\mathrm{o}/\partial \theta$, and using this in (2.3) and integrating by parts gives

$$E_\mathrm{o}(y) = -c_\mathrm{o} \int \theta \, \mathrm{d}\Psi_\mathrm{o} = c_\mathrm{o} \int \Psi_\mathrm{o} \mathrm{d}\theta \sim \Psi_{\mathrm{o,max}} S_\mathrm{o}. \tag{2.4}$$

That is, the energy transport is, very roughly, the magnitude of the overturning stream function Ψ_o multiplied by the gross stability of the ocean S_o.

In the atmosphere, the corresponding circulation is the thickness-weighted overturning circulation with respect to moist static-energy surfaces (the 'energy transport stream function'; Czaja and Marshall, 2006). This will resemble, but not in general be equal to, the more familiar thickness-weighted residual circulation. If the energy transport stream function is denoted by Ψ_a, then the meridional heat transfer in the atmosphere is given, by definition, by

$$E_\mathrm{a}(y) = -\int S_\mathrm{m} \, \mathrm{d}\Psi_\mathrm{a} = \int \Psi_\mathrm{a} \, \mathrm{d}S_\mathrm{m} \sim \Psi_{\mathrm{a,max}} S_\mathrm{a}. \tag{2.5}$$

We will give details of our numerical experiments later on, but it will help to motivate the scaling theory to

DOI: 10.1002/qj

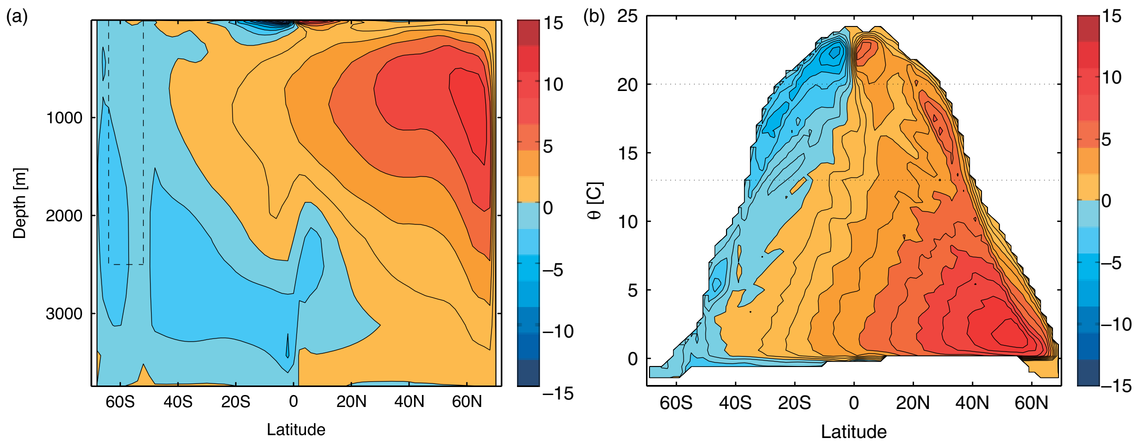

Figure 1. The overturning circulation of the ocean in our control integration, in (a) physical space and (b) 'potential temperature space'. The horizontal dashed lines show the demarcation between the two warm cells and the cold deep cell used in the energy transport calculations. Units are Sverdrups: 1Sv $= 10^9$kg s^{-1}.

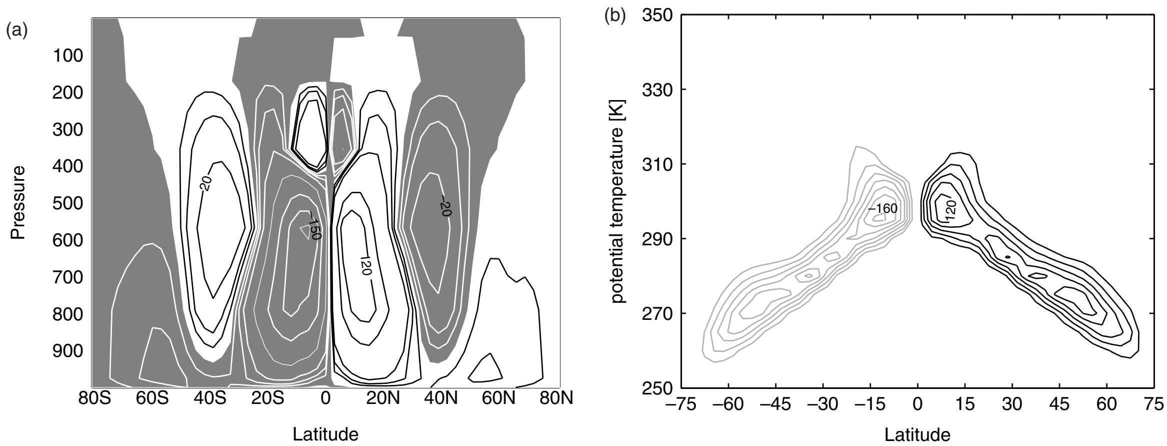

Figure 2. The overturning circulation of the atmosphere in our control integration: (a) the Eulerian circulation in physical space; (b) the residual circulation in potential temperature space. Units are Sverdrups: 1Sv $= 10^9$kg s^{-1}.

look now at the overturning circulation of our standard simulation, shown in Figures 1 and 2 respectively. (The atmospheric values are multiplied by three, because the longitudinal extent of the model is 120°.) The atmospheric heat transport is effected by a direct, quasi-steady Hadley cell in low latitudes. (In these simulations there is also a weak, counter-rotating cell in the upper tropical troposphere that has little effect on the heat transport.) In midlatitudes baroclinic eddies effect most of the transfer, and the residual circulation differs markedly from the Eulerian circulation. The strength of the circulation is similar to, albeit somewhat stronger than, the observed annual average, although the vertical extent of the Hadley cell is not as great as observed, and so it is not potentially warm at its top (note that the model has no seasonal cycle and a poor stratosphere).

In the ocean the overturning circulation comprises a deep overturning cell as well as shallow, warm cells. With sufficiently small diapycnal diffusivity, these cells are reasonably well separated and arise from fairly distinct processes, although the cells may nevertheless interact. The deep cell is both diffusively driven (with an advective–diffusive balance in the main thermocline) and mechanically driven by winds, especially those in the Southern Ocean. The shallow cells are primarily wind-driven, comprising the flow in both the great gyres and the Ekman layers.

3. Ocean energy transport

We may divide the ocean circulation into the following components:

(i) energy transport in the wind-driven gyres, including the Ekman layer and upper thermocline;
(ii) energy transport in the diffusively driven meridional overturning circulation (MOC);
(iii) energy transport in the mechanically driven MOC, i.e. the MOC driven by zonal winds in the Southern Hemisphere circumpolar channel.

We will largely ignore the effects of mesoscale eddies and suppose that the circulation is steady. We also note that the ratio of the Sverdrup transport, M_S, to the Ekman transport, M_E, increases with latitude (Pedlosky, 1996); only at low latitudes is the ratio smaller than one, and

DOI: 10.1002/qj

because our focus is the extratropics we will not explicitly consider the Ekman transport further.

3.1. Heat transport in wind-driven gyres

In subtropical wind-driven gyres, the heat transport occurs because the water moving polewards in the western boundary current is warmer than the water moving equatorwards elsewhere in the gyre. We may pursue a crude estimate by assuming that that the gyre is quasi-two-dimensional, as motivated by Figure 1, which indicates that the poleward and equatorward flow occur at similar levels, and as addressed in an ocean-only context by Bye and Veronis (1980) and Wang *et al.* (1995) with a specified thermal relaxation coefficient. In a coupled model with an interacting atmosphere, the thermodynamic relaxation time of the upper ocean cannot be controlled and we take an even more phenomenological approach. Let us assume that the heat flux is given by the product of the gyre mass flux with a temperature difference, multiplied by the heat capacity. If the mass transport is given by Sverdrup balance, a crude scaling for the energy flux in a gyre, E_{g}, is then

$$E_{\mathrm{g}} \sim \frac{\tau^x L_x}{\beta L_y} c_{\mathrm{o}} \Delta\theta_{\mathrm{o}}, \tag{3.1}$$

where τ^x is the surface zonal wind stress (we will subsequently drop the superscript and take the stress always to be zonal), L_x is the zonal extent of the basin, L_y the meridional scale of the gyre and $\Delta\theta_{\mathrm{o}}$ the temperature difference between polewards- and equatorwards-flowing water, an upper estimate for which would be the meridional temperature difference across the subtropical gyre.

We might try to improve on (3.1) by noting that, in the Sverdrup interior, the flow is sluggish and to first approximation the near-surface temperature will be similar to the average temperature of the atmosphere at that latitude, $\bar{\theta}(y)$ say. In contrast, in a vigorous polewards-flowing western boundary current the surface temperature is warmer than the average, and we might suppose it obeys an equation like $\mathrm{d}\theta/\mathrm{d}t = -\lambda\big[\theta - \bar{\theta}(y)\big]$ where λ is approximately constant and in a quasi-steady state $\mathrm{d}/\mathrm{d}t \sim v\,\mathrm{d}/\mathrm{d}y$. (This balance was invoked by Wang *et al.* 1995.) Depending on the value of λ, the temperature $\theta(y)$ lies between its value at the entrance to the western boundary current, $\theta(y_{\mathrm{s}})$ (where y_{s} is the latitude of the entrance to the western boundary current), and the value of $\bar{\theta}(y)$. With a very intense western boundary current the temperature in the current is just $\theta(y_{\mathrm{s}})$ because it does not get the chance to cool significantly, and also $\theta(y_{\mathrm{s}}) \approx \bar{\theta}(y_{\mathrm{s}})$. An upper estimate for the energy transport in the subtropical gyre is then

$$E_{\mathrm{g}}(y) \sim \frac{c_{\mathrm{o}} \tau L_x}{L_y \beta}[\bar{\theta}(y_{\mathrm{s}}) - \bar{\theta}(y)]. \tag{3.2}$$

In this efficient limit the energy transport depends linearly on the wind stress and linearly on the basin width, but these are not the only possibilities (as discussed by Bye and Veronis (1980) and Wang *et al.* (1995)), because $\Delta\theta_{\mathrm{o}}$ can change with the wind strength. Wang *et al.* considered two limits depending on the thermal relaxation coefficient: as $\lambda \to \infty$ ($\lambda \to 0$) they predict that the heat transfer depends on τ^2 (τ^0). In addition, as the width of the domain increases, the Sverdrup transport increases but the boundary-layer width does not; thus the velocity in the western boundary current must increase, potentially further increasing the heat transfer until such time as the western boundary current is isothermal and the efficient limit is reached. Prior to reaching that limit, the heat transfer would increase more than linearly with basin width.

The precise behaviour of the heat transport will in general depend on whether the western boundary current is a Stommel layer (with linear drag) or a Munk layer (with harmonic friction), or something else. In reality the real western boundary current is some combination further complicated by the effects of stratification, topography and nonlinearity and (3.2) must therefore be regarded as an approximate estimate. In spite of this, the above arguments have some robust aspects. They suggest that the heat transport will be small at the equatorial edge of the gyre, and increase slowly polewards as the temperature difference between the western boundary current and the equatorwards Sverdrup flow increases, before falling more quickly at the poleward edge of the gyre. Furthermore, as β increases then the scaling predicts that heat transport will diminish for a given wind stress, other factors remaining the same. Finally, the gyral energy transport will depend on the surface winds, and thus directly on the intensity of the circulation in the atmosphere.

3.2. Heat transport by a diffusively controlled deep circulation

Classical scaling (Robinson and Stommel, 1959; Welander, 1986; Vallis, 2006) suggests that in a single hemisphere the diffusion-controlled overturning stream function Ψ_{d} scales as

$$\Psi_{\mathrm{d}} \sim \kappa_{\mathrm{v}}^{2/3} \left(\frac{\Delta b L_y}{f}\right)^{1/3}, \tag{3.3}$$

having simplified by taking $\beta \sim f/L_y$, and where Δb is the meridional buoyancy difference across the hemisphere, κ_{v} is the diapycnal diffusivity and L_y is the meridional extent of the basin. With a linear equation of state and no salinity – an oversimplification in the real world – Δb is related to a temperature difference by $\Delta b \approx g\beta_{\mathrm{T}}\Delta\theta$, where β_{T} is a thermal expansion coefficient. In the presence of wind, the scaling for the strength of the circulation differs somewhat (Samelson and Vallis, 1997), becoming

$$\Psi_{\mathrm{d}} \sim \kappa_{\mathrm{v}}^{1/2} \left(\frac{\Delta b\, L_y^2 W_{\mathrm{E}}}{f}\right)^{1/4}, \tag{3.4}$$

where W_{E} is the vertical velocity due to Ekman pumping and Δb is the buoyancy difference across the subpolar gyre. (In the case with an inter-hemispheric overturning circulation, the buoyancy difference is related to the temperature difference between the hemispheres, but the theory is not settled in this case.) The equatorwards-flowing water has a near-constant temperature of sinking water near the Pole, $\bar{\theta}(y_p)$, and if the polewards-flowing return water has a temperature $\bar{\theta}(y)$ the associated heat transfer is

$$E_d(y) \sim c_o \rho_o \Psi_d[\bar{\theta}(y) - \bar{\theta}(y_p)]L_x. \quad (3.5)$$

The polewards-flowing water is partially shielded from the surface by the near-isothermal base of the ventilated thermocline, and so at low latitudes its temperature will approximately equal the surface temperature of the surface at the boundary between the subtropical and subpolar gyres. In any case, one may expect the heat transport to be small at the highest latitudes where $\bar{\theta}(y) \approx \bar{\theta}(y_p)$, increasing fairly rapidly equatorwards as the temperature contrast between $\bar{\theta}(y)$ and $\bar{\theta}(y_p)$ increases, and then diminishing more slowly equatorwards as the cell passes under the polewards edge of the subtropical gyre and the intensity of the deep cell falls (numerical simulations are illustrated in Figure 7 later).

To obtain a useful scaling estimate of the overall magnitude of energy transport, we can combine (3.5) and (3.4) to give

$$E_{do} \propto \kappa_v^{1/2} \Delta\theta^{5/4} f^{-1/4} L_x, \quad (3.6)$$

where we simply take $\Delta\theta$ to be proportional to the meridional temperature difference across the hemisphere. Given the various idealizations made in the derivation (including the omission of a treatment of salinity), (3.6) cannot be regarded as at all precise, but robust predictions are that the heat transport will increase rather slowly with the diapycnal diffusivity and have a weak dependence on Coriolis parameter.

3.3. Heat transport by the mechanically driven, inter-hemispheric MOC

If the southern end of the domain is zonally periodic, then an inter-hemispheric mechanically driven MOC can be set up with a strength determined, at least in part, by the zonal wind over the circumpolar channel, as sketched in Figure 3 (Eady, 1957; Toggweiler and Samuels, 1998; Gnanadesikan, 1999; Vallis, 2000; Samelson, 2004). The mass transport, $\rho\Psi_{Ek}$ in the Ekman layer of the circumpolar channel is given by

$$\rho\Psi_{Ek} = \frac{1}{f}\tau. \quad (3.7)$$

If we envision a circulation like that of Figure 3, then the southwards-flowing water has the properties of the flow that sinks at high northern latitudes. If the northward flow takes on the temperature at the surface, and the southward flow has the temperature $\bar{\theta}_n$ of high northern latitudes, then the associated heat transport is given by

$$E_{Ek} \sim c_o \rho_o \Psi_{Ek} \Delta\theta L_x = \frac{c_o}{f_C}\tau_C[\bar{\theta}(y) - \bar{\theta}_n]L_x. \quad (3.8)$$

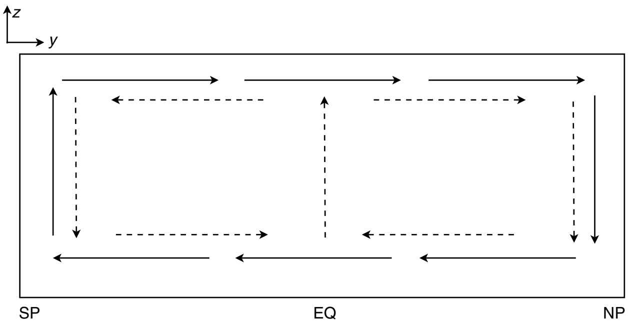

Figure 3. Schematic of a putative MOC that is driven by winds in the southern circumpolar channel (solid arrows) and by buoyancy gradients and diapycnal mixing (dashed arrows). The two circulations reinforce in the Northern Hemisphere, but tend to cancel in the Southern Hemisphere.

where f_C and τ_C are, respectively, the value of the Coriolis parameter and the wind stress in the circumpolar channel. In this model, the heat flux is *northwards* in both hemispheres, and takes approximately the same value at each pair of latitudes, to the extent that the temperatures at each latitude are approximately the same in each hemisphere. Thus, blocking the Drake Passage may be expected to increase the polewards energy transport in the Southern Ocean and decrease it by a similar amount in the Northern Hemisphere.

In the Southern Ocean, the heat transport of the mechanically driven MOC is in the opposite direction to that of the diffusively driven MOC. Using (3.3) and (3.7), a non-dimensional number that indicates their relative importance is the ratio of their mass transports:

$$\alpha = \frac{\Psi_{Ek}}{\Psi_d} \sim \frac{\tau_C/\rho}{\left(\kappa_v^2 \Delta b L_y f_C^2\right)^{1/3}}. \quad (3.9)$$

If $\alpha \gg 1$, then mechanically driven overturning will dominate and the heat transport of the Southern Ocean will be northward. If $\alpha \ll 1$ then diffusively driven overturning will dominate, and the heat transport will be poleward, and hence southward. Observations show that in the South Atlantic the net oceanic energy transport is in fact northwards and of a similar magnitude to the polewards transport in the North Atlantic (Trenberth and Caron, 2001), suggesting that the wind-driven component is slightly larger than the diffusively driven component.

4. Atmospheric heat transport

Heat transport in the atmospheric midlatitudes must involve a theory of large-scale turbulence and, because such theories are inexact, a scaling of that transport will be approximate. However, because it is the same baroclinic eddies that transport energy polewards as produce the surface winds that drive the ocean circulation, it may be possible to produce an estimate of the partitioning of the transport between the atmosphere and wind-driven ocean circulation without solving the turbulence problem itself.

DOI: 10.1002/qj

In midlatitudes the dry static-energy flux is approximately equal to the potential temperature flux, and we suppose that the potential temperature flux is diffusive with

$$\overline{v'\theta'} = -\kappa_{\mathrm{a}} \frac{\partial \bar{\theta}}{\partial y}, \tag{4.1}$$

where κ_{a} is some quasi-horizontal diffusivity due to the large-scale baroclinic eddies in the atmosphere. The total polewards transfer of dry static energy by eddies is then

$$E_{\mathrm{da}} = -\int \rho_{\mathrm{a}} c_p \left(\frac{T}{\theta}\right) \kappa_{\mathrm{a}} \frac{\partial \bar{\theta}}{\partial y} \mathrm{d}x \mathrm{d}z \sim \rho_{\mathrm{S}} c_p H_{\mathrm{a}} \frac{\hat{L}_x}{L_y} \kappa_{\mathrm{a}} \Delta\theta_{\mathrm{a}}, \tag{4.2}$$

where $\hat{L}_x$ is the zonal extent of the atmosphere, H_{a} is a vertical scale, L_y is the width of the baroclinic zone and the quantity $\Delta\theta_{\mathrm{a}}$ is the temperature difference across midlatitudes. (There are potentially multiple vertical scales in the problem – a density scale height, an eddy scale height etc. We assume they are similar.) The parameter ρ_{S} is a density scaling value and $\rho_{\mathrm{S}} \sim P_{\mathrm{s}}/gH_{\mathrm{a}}$ where P_{s} is the surface pressure.

Water vapour is transferred polewards by these same eddies, although the bulk of the transfer may occur even lower in the troposphere, as the upper midlatitudes are relatively dry. If the relative humidity, r, is nearly constant then the moisture flux is related to the temperature flux by

$$\overline{v'q'} \approx r \frac{\partial \mathrm{q_s}}{\partial T} \overline{v'T'} \approx r \frac{\partial \mathrm{q_s}}{\partial T} \left(\frac{T}{\theta}\right) \overline{v'\theta'}. \tag{4.3}$$

Expressions similar to this are common in the literature – see for example Leovy (1973) and Stone and Yau (1990). Undoubtedly, such a local relation is imperfect and, given the presence of condensation diffusive parametrizations in general, cannot properly be justified (Vallis, 1982; O'Gorman and Schneider, 2006). Caballero and Langen (2005) and O'Gorman and Schneider (2008) in fact found somewhat complicated behaviour in the hydrological cycle as climate changes, and Pierrehumbert *et al.* (2006) provide a discussion of the general issue.

The robust expectation of the above argument is that if the atmosphere warms or the moisture content of the atmosphere otherwise increases then the fraction of the atmospheric energy transfer due to water vapour will increase, roughly following Clausius–Clapeyron scaling, and this behaviour was approximately found to occur in comprehensive GCMs by Held and Soden (2006). Other things remaining the same, one might expect to see a decrease in the meridional flux of sensible heat in order to keep the total energy transport constant – a 'compensation'. However, if there is natural variability of the climate system caused by, for example, oceanic variability on decadal time-scales with little change in mean temperature, then one might expect to see the dry static energy and the moisture flux vary in unison, because of the proportionality in (4.3); this hypothesis will be tested in future work.

A large cause of uncertainty in the above estimates is the eddy diffusivity itself, κ_{a}. No widely accepted theory exists, certainly in the presence of moisture, and although quasi-geostrophic theories of heat fluxes (Held and Larichev, 1996) suggest that κ_{a} will increase rapidly with $\Delta\theta$, the vertical heat flux may also increase with horizontal temperature gradient, reducing the need for large increases in horizontal fluxes to stabilize the flow (Gutowski, 1985; Gutowski *et al.*, 1989), as found in the simulations of Schneider and Walker (2008). Still, in a full GCM Barry *et al.* (2002) find a somewhat faster than linear increase of heat flux with temperature gradient, and in a two-level primitive equation model Zurita-Gotor and Vallis (2009) find that both horizontal and vertical heat fluxes increase rapidly with meridional temperature gradient. The overall uncertainty suggests that we should try to construct theories of partitioning between the ocean and atmosphere that are independent of κ_{a}.

4.1. Surface wind

In midlatitudes the mean surface stress, τ, is a response to the eddy momentum convergence in baroclinic eddies. In general the momentum flux convergence may be expressed as the sum of contributions from a potential vorticity flux in the interior and a buoyancy flux at the boundaries. Green (1970) suggested that the potential vorticity and heat fluxes be parametrized diffusively, obtaining a closed expression for the surface winds, assumed to be linearly proportional to the surface stress (see White and Green (1984), Gallego and Cessi (2000) and Cessi (2000) for more discussion). The expression for the surface stress is complicated, but given a diffusive approximation a scaling for its magnitude has the form

$$|\tau| \sim \int \kappa_{\mathrm{a}} \rho_{\mathrm{a}} \frac{\partial \bar{Q}}{\partial y} \mathrm{d}z \sim \kappa_{\mathrm{a}} \frac{\beta P_{\mathrm{s}}}{g}, \tag{4.4}$$

where κ_{a} is an eddy diffusivity and P_{s} is the mean surface pressure. The gradient of potential vorticity has contributions from β, the curvature of the wind and the meridional temperature gradient, but if the β effect is the dominant external agent determining the lateral potential vorticity gradient in the free atmosphere then the second estimate on the right-hand side of (4.4) results. The scaling is crude, but if it is in fact the eddy diffusivity κ_{a} that changes most as parameters such as the Pole – Equator temperature gradient vary, then the magnitude of changes in the surface stress can be related to changes in the atmospheric heat transport using (4.1) and (4.4).

5. Partitioning between the atmosphere and ocean

5.1. The atmosphere and the wind-driven ocean circulation

Combining (3.1) and (4.4), a crude scaling for the energy transport in a wind-driven ocean gyre is given by

$$E_{\mathrm{g}} \sim \frac{\kappa_{\mathrm{a}} P_{\mathrm{s}} L_x}{g L_y} c_{\mathrm{o}} \Delta\theta_{\mathrm{o}}, \tag{5.1}$$

where L_x is the width of the basin and $\Delta\theta_{\mathrm{o}}$ the temperature difference across it. From (4.2), the dry static-energy transport in the atmosphere is

$$E_{\mathrm{da}} \sim \frac{P_{\mathrm{s}} c_p \hat{L}_x}{g L_y} \kappa_{\mathrm{a}} \Delta\theta_{\mathrm{a}}. \tag{5.2}$$

The ratio of the above two expressions is

$$\frac{E_{\mathrm{da}}}{E_{\mathrm{g}}} \sim \frac{c_p \Delta\theta_{\mathrm{a}}}{c_{\mathrm{o}} \gamma \Delta\theta_{\mathrm{o}}}, \tag{5.3}$$

where γ is the ratio of the zonal dimensions of the ocean and atmosphere and $\Delta\theta_{\mathrm{a}}$ and $\Delta\theta_{\mathrm{o}}$ are the gross temperature differences seen by the two media. If we include the effects of water vapour in the atmospheric transport, then the ratio of atmospheric to gyral energy transfer is given by

$$\frac{E_{\mathrm{a}}}{E_{\mathrm{g}}} \sim \frac{(c_p + rL\partial q_{\mathrm{s}} T)\Delta\theta_{\mathrm{a}}}{c_{\mathrm{o}} \gamma \Delta\theta_{\mathrm{o}}} \sim \frac{c_p \Gamma_{\mathrm{d}} \Delta\theta_{\mathrm{a}}}{c_{\mathrm{o}} \gamma \Gamma_{\mathrm{m}} \Delta\theta_{\mathrm{o}}}, \tag{5.4}$$

where Γ_{m} and Γ_{d} are the moist and dry lapse rates, and the rightmost expression holds if $r \approx 1$ (see Held, 2001). The result implies that the ratio of the heat transports of the two subsystems will scale as the ratio of their respective gross stabilities, essentially because the mass transports scale the same way (although the mass transport of the atmosphere generally exceeds that of the ocean in mid and high latitudes). Thus, in the absence of changes in the structure of the two subsystems, we may expect that as external parameters (such as the distribution of incoming solar radiation) vary the heat transports of the atmosphere and the oceanic gyres will change proportionally. The proportionality holds in the efficient limit in which the western boundary current is quite intense; if the flow is less intense, then the ocean's heat transport may increase faster than linearly with wind stress (Wang *et al.*, 1995).

A consequence of the above arguments is that the atmospheric heat transport and wind-driven ocean transport are predicted to vary more-or-less in unison on long (e.g., decadal) time-scales, with the atmospheric variations leading those of the ocean, because the gyres are largely driven by the atmosphere. However, the correlation between the total heat transport of the ocean and that of the atmosphere is likely to be negative on those time-scales, as the atmosphere seeks to compensate for slow natural variability in the deep ocean.

Having said all this, the chain of reasoning leading to (5.4) is long, and there are inaccuracies in the atmospheric transport (perhaps especially in the treatment of moisture) and the surface wind expression (through the use of a diffusive approximation for potential vorticity) and in the barotropic, quasi-two-dimensional, treatment of the ocean.

5.2. The atmosphere and the buoyancy-driven ocean overturning

If we take the oceanic diapycnal diffusivity as given, then we may obtain an estimate for the ratio of the atmospheric heat transport E_{a} to the diffusively driven oceanic heat transport E_{B}, using (4.2) and (3.6). The full expression is uninformative, but, omitting a number of geometric terms and physical constants, the ratio of the atmospheric heat transport, E_{a}, to the buoyancy-driven ocean heat transport, E_{B}, scales as

$$\frac{E_{\mathrm{a}}}{E_{\mathrm{B}}} \sim \frac{\kappa_{\mathrm{a}} \Delta\theta_{\mathrm{a}}}{\kappa_{\mathrm{v}}^{1/2} \Delta\theta_{\mathrm{o}}^{5/4} \gamma}. \tag{5.5}$$

The expression involves the horizontal baroclinic-eddy diffusivity of the atmosphere, κ_{a}, and the vertical diapycnal diffusivity of the ocean, κ_{v}, and for neither of these is there an accepted theory. We cannot, therefore, state that the atmospheric energy transport can a priori be expected to be larger than that of the ocean. If the ocean basins were wider, and if the diapycnal diffusivity of the ocean were larger, there seems to be no reason that the oceanic heat transport could not be larger than that of the atmosphere, although the oceanic diffusivity, κ_{v}, almost certainly depends on the intensity of atmospheric circulation.

6. Numerical experiments

In the remainder of this article we describe some numerical experiments that we use to explore the meridional energy transport. Our model is a coupled atmosphere–ocean–ice–land model similar to current state-of-the-art coupled general circulation models, but idealized in two main ways: the physical parametrizations of the atmosphere and the general geometry and geography of the model are simplified in comparison with a more comprehensive climate model, as described in more detail in Farneti and Vallis (2009). The atmospheric model is a moist, hydrostatic, gridded, three-dimensional primitive equation model, using the physical parametrizations of Frierson *et al.* (2006), but with a longitudinal extent of 120° and zonally periodic boundary conditions. The horizontal resolution is approximately 3.5°, increasing to 1.5° to test convergence at higher rotation rates. The ocean model is a free-surface primitive equation model in z-coordinates. The main simplification is that there is a single basin, which in our control configuration is 60° wide, extending from 70°S to 70°N. The basin is enclosed on all four sides, except that in our control calculation in the region from 65° – 51°S the walls are removed and cyclic boundary conditions are imposed (i.e., the zonal

DOI: 10.1002/qj

flow is re-entrant), thus crudely representing the Antarctic Circumpolar Channel (ACC). The horizontal resolution is approximately 2°, there are 24 vertical grid points, and the ocean is flat-bottomed with a depth (in the control simulation) of 4000 m, except in the model Drake Passage where the depth is 2500 m. A simple land model returns precipitation to the ocean. For each experiment we integrate the coupled model to equilibrium, which may take 1000 years or more, and then take averages over an additional 100 years.

6.1. Energy transport in the control integration

The atmospheric, oceanic and total meridional energy transport in the control integration and in observations are shown in Figures 4 and 5. Because our model is only 120° in longitudinal extent, in Figure 4 we multiply our transports in both atmosphere and ocean by a factor of three for comparison with observations. The aspects that stand out, in both observations and model, and a brief explanation for each, are as follows.

(1) The gross similarity in the magnitude of the energy transports of the ocean and atmosphere: the magnitudes of the two transports are generally within a factor of a few of each other and do not differ by an order of magnitude.
The gross stability of the atmosphere and, especially, its mass transport are larger than that of the ocean and this accounts for its larger energy transport in midlatitudes. However, as noted above, there is no a priori reason that a wide ocean, or a very diffusive ocean, could not transport more heat than the overlying atmosphere, as we in fact find later.

(2) The larger transport of the ocean at very low latitudes, at least in the Northern Hemisphere, and the dominance of the atmosphere at mid and high latitudes.
As noted previously the atmospheric heat transport is expected to be small at the Equator but increase with latitude, whereas the tropical gyre transport is large at the Equator – larger than that of the atmosphere – but falls with latitude. In midlatitudes the wind-driven subtropical gyre and the deep overturning are responsible for the oceanic component but are less than that of the atmosphere, for the reasons noted above.

(3) The relatively small oceanic transport in the Southern Hemisphere.
The wind-driven overturning circulation, driven by Southern Ocean winds, produces a northward heat transfer, whereas the diffusively driven component produces a poleward heat transfer in both hemispheres (see Figure 3). The heat transfer in the Southern Ocean will therefore be smaller than that in the North to an extent determined by the value of the diapycnal diffusivity and Southern Hemisphere winds.

The atmospheric transport may be further divided into contributions from the dry static energy and from moisture (not shown). The total (moist static energy) transport is slightly larger in the Southern Hemisphere, partially compensating for the weaker ocean transport in the Southern Hemisphere, resulting in a total (atmosphere plus ocean) transport that is nearly, but not exactly, the same in both hemispheres.

The oceanic heat transport is nearly all advective and, apart from the ACC region where the bolus advection by the mesoscale eddy parametrization (a 'GM' scheme, following Gent and McWilliams, 1990) is important, it is nearly all accomplished by the mean advection – that is, by the resolved flow. We decompose this transport into an 'overturning' circulation and a 'gyre' circulation using isentropic coordinates, as in (2.4), and motivated by Figure 1 the ocean heat transport (OHT) in the various cells is then defined as

$$OHT = c_o \int_{\theta_1}^{\theta_2} \Psi_o \, d\theta, \qquad (6.1)$$

where $(\theta_1, \theta_2) = (20^\circ, 25^\circ)$ for the tropical cell, $(13^\circ, 20^\circ)$ for the midlatitude or intermediate cell and $(0^\circ, 13^\circ)$ for the cold overturning cell, as seen in Figure 1. Although the partitioning is a little arbitrary, the contributions of the three cells are fairly clearly delineated, and changing the cell boundaries by small amounts made little difference. The results are shown in Figure 7. The gyre contributions are almost symmetric across the Equator and roughly follow the patterns described previously, whereas the overturning circulation is much smaller in the Southern Hemisphere than in the Northern Hemisphere, reflecting the cancellation of the wind-driven and diffusively-driven components.

7. Effects of ocean geometry

We now describe experiments in which aspects of the geometry of the ocean are changed. We change the depth of the ocean, its width, whether or not it is contained by meridional walls, and whether or not there is a periodic channel at the southern end of the ocean, representing the ACC and Drake Passage. The gross effects of some of these changes on the meridional overturning circulation of the ocean can be seen in Figure 6, and in what follows we discuss the individual changes in more detail.

7.1. Closing the circumpolar channel

Our control simulation has a periodic channel at the southern edge of the ocean basin, representing the ACC. In past times it is likely that the Drake Passage – the opening between the southern tip of South America and the Antarctic Peninsula – was closed. Although this is superficially only a small change to the global geometry of the ocean, it has been suggested or found in other simulations that blocking Drake Passage could have significant effects on the ocean circulation (Toggweiler

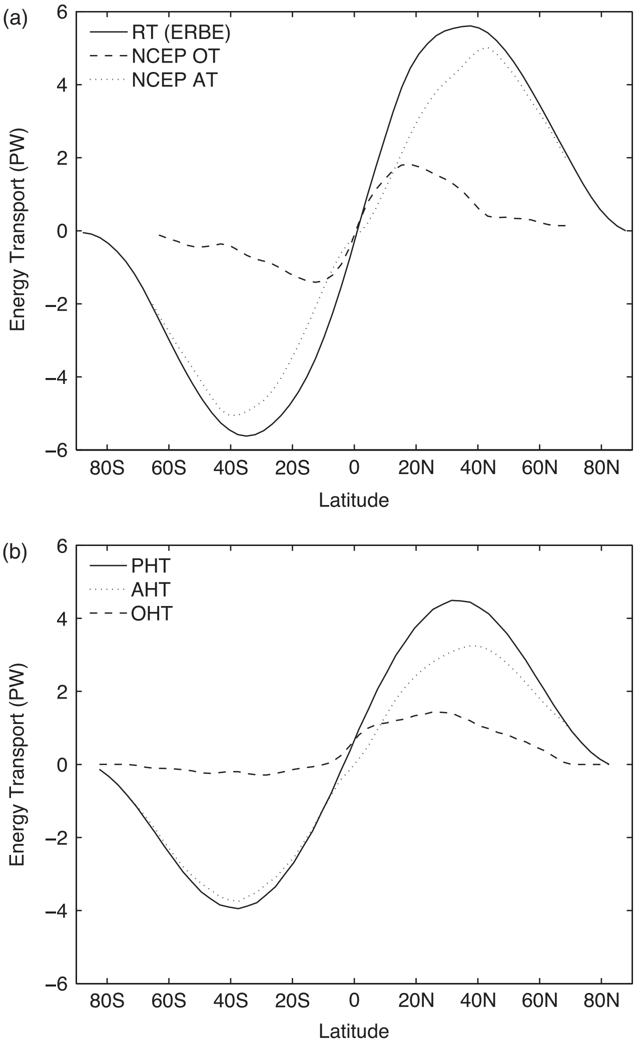

Figure 4. (a) Observed/reanalysed meridional energy transfer in the atmosphere, ocean and their sum (RT), using data from Trenberth and Caron (2001). (b) The modelled energy transfer in the control integration, times 3. AHT, OHT and PHT refer to atmospheric, oceanic and planetary (the sum) heat transport.

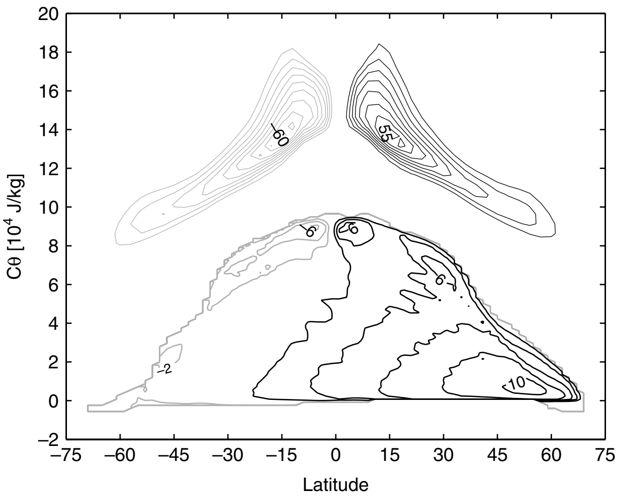

Figure 5. The energy-residual overturning circulation in the atmosphere and ocean in our control integration. The ordinate is the respective energy coordinate for the atmosphere (upper contours) and ocean (lower contours). The ocean and the atmosphere both span a similar range of energy (the ordinate), but the atmospheric circulation is stronger.

and Samuels, 1998; Gnanadesikan, 1999; Vallis, 2000; Sijp and England, 2004; Enderton and Marshall, 2009). Given hemispherically symmetric geometry and forcing, the meridional overturning circulation transports energy polewards in both hemispheres. When the Drake Passage is opened, an additional 'wind-driven' overturning circulation transports energy northwards in *both* hemispheres.† There is then a cancellation between the wind-driven and diffusive MOCs and the net heat transport is much reduced, whereas in the Northern Hemisphere opening the model Drake Passage serves to *increase* the polewards energy transport, as in Figure 8.

Note that the presence of a southern circumpolar channel reduces the meridional energy transport in the Southern Hemisphere, not so much by blocking the meridional overturning circulation, or by changing the wind-driven gyres, but by enabling a wind-driven

†Both wind and buoyancy gradients are important in maintaining this circulation, and we refer to it as 'wind-driven' to differentiate it from the classical overturning circulation (the 'diffusive MOC'), which is maintained by buoyancy gradients and mixing.

DOI: 10.1002/qj

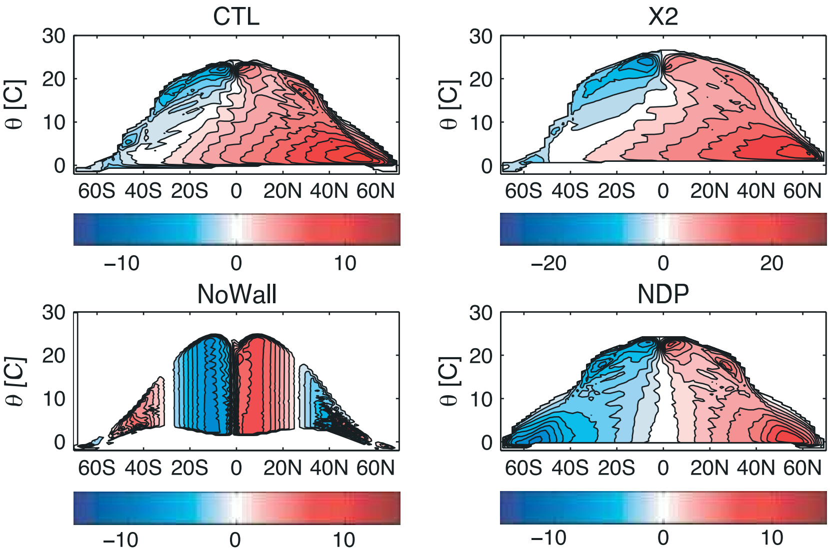

Figure 6. Meridional overturning circulation (MOC) in experiments with different ocean geometries. '×2' means the ocean basin width is double that of the control, 'No Wall' means the ocean has zonally periodic boundary conditions at all latitudes, NDP means than the Drake Passage is blocked. Contours are in units of 1 Sv except for ×2 where the interval is 3 Sv.

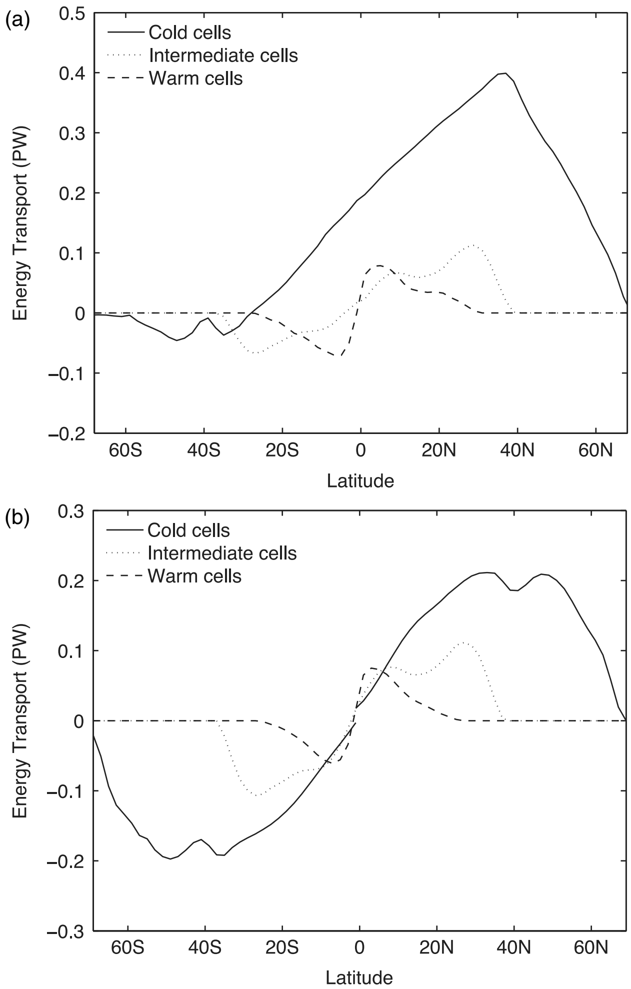

Figure 7. (a) Overturning and gyre components of oceanic meridional heat transport in the control simulation, with a circumpolar channel in the Southern Hemisphere. 'Cold cells' is essentially the deep overturning circulation, 'intermediate cells' the subtropical gyres and 'warm cells' the tropical cells. (b) The same but for a simulation with no circumpolar channel, and hence with near-symmetry across the Equator.

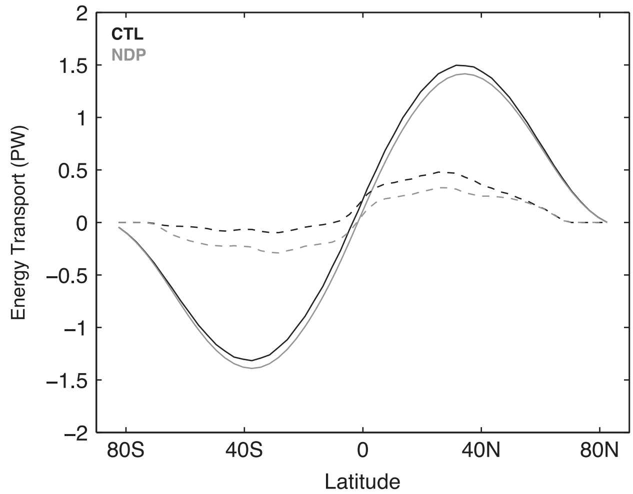

Figure 8. Oceanic meridional energy transport (dotted lines) and the total (atmospheric plus oceanic) energy transport (solid lines) in simulations with and without a zonally periodic circumpolar channel. The lighter lines, denoted NDP (No Drake Passage), are for the simulations with no channel and are almost symmetric about the Equator.

overturning circulation that partially cancels the diffusive circulation: even in subtropical latitudes the southward energy transport in the case with the circumpolar channel is much reduced.

7.2. Changing the ocean depth and width

Simple theory (section 3.1 and 3.2) suggests that neither the heat transport in the diffusively driven deep overturning circulation nor the Sverdrupian mass transport of the wind-driven circulation should depend on the ocean depth, provided that depth is greater than that to which the Sverdrupian flow naturally penetrates. This approximately corresponds to the depth of the main thermocline, i.e, about 500–800 m, and this is determined by the strength of the wind, the buoyancy contrast across the gyre and the diapycnal diffusivity (which may be regarded as affecting the thermocline 'thickness'; Samelson and Vallis, 1997). If the ocean is shallower than this depth then we can expect both the overturning circulation and the gyre dynamics and its heat transport to be modified, and the scaling estimates may fail, although even then the Sverdrup transport will not necessarily decrease unless bottom drag plays an important role.

We have tested these expectations by performing a series of experiments with oceans of different depths, using a hemispherically symmetric configuration (i.e. with no circumpolar channel in the Southern Hemisphere) for simplicity. The depth of the ocean in our control simulation is 4000 m, and in addition to this we have performed experiments with a base ocean depth of 2000 m, 1000 m, 500 m and 50 m; the last one represents the ocean as a slab mixed layer, and provides no horizontal transport. The oceanic meridional circulations can be seen in Figure 10, and the ocean heat transport itself is plotted in Figure 9. In these and similar plots the atmospheric heat transfer is a time and space average over latitudes from 20°–60°, and the oceanic heat transport is generally a peak value over the particular cell or over the entire ocean; the results are not sensitive to the convention used.

The oceanic meridional heat transport generally varies rather little as the ocean depth changes (Figure 9), provided the depth is greater than that of the main thermocline. In fact, the energy transport actually increases slightly as the ocean depth diminishes, this being caused by an intensification of the deep overturning circulation (Figure 10). The increase is relatively modest, and as soon as the ocean depth is less than that of the main thermocline (about 700 m) the changes are much more apparent. The wind-driven circulation then directly feels the bottom of the ocean and the transport in the warm cells diminishes. The atmosphere compensates quite well for changes in the ocean energy transport, and the total meridional energy transport is almost constant as ocean depth changes. This remains true even as the dynamical ocean is replaced by a slab mixed layer and no lateral transport, marked by the dots at 50 m in Figure 9.

Changing the width of the ocean basin is expected to, and does, change the meridional heat transport of the ocean, and the effect is somewhat more than linear (open circles in Figure 9) because the western boundary current becomes more intense. The atmospheric heat transport in the wide ocean case is reduced, and in fact it is now *less* than that of the ocean, but the compensation is by no means perfect and the total heat transport of the atmosphere and ocean is noticeably increased with a wider ocean.

7.3. Removing the meridional walls of the ocean

A profound change to the ocean circulation results if the meridional walls are removed and replaced with zonally cyclic conditions, in a configuration similar to that of Marshall *et al.* (2007) and Enderton and Marshall (2009).

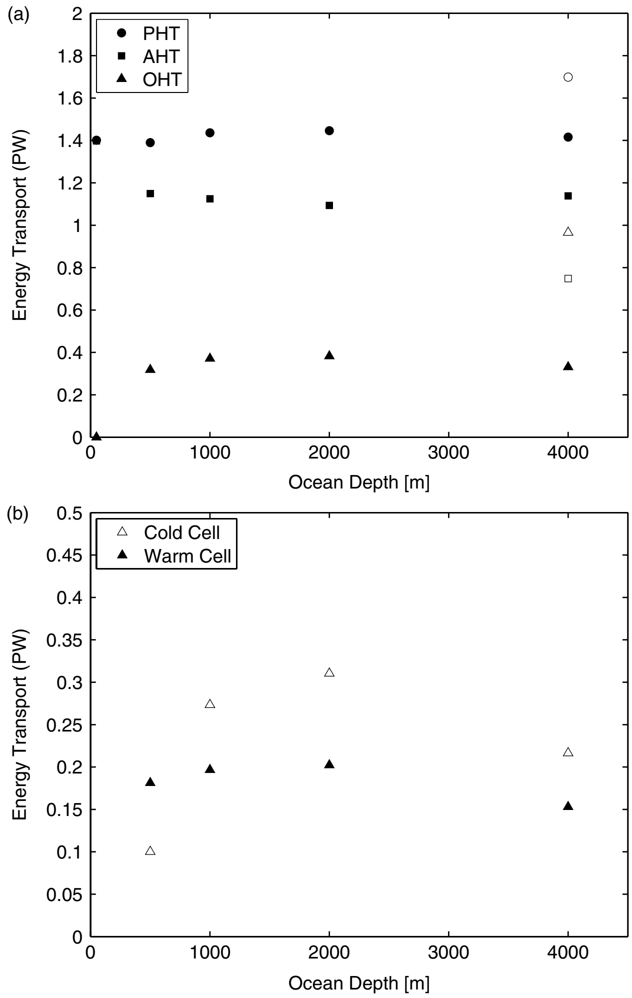

Figure 9. (a) Midlatitude atmospheric, oceanic and planetary energy transport (AHT, OHT and PHT respectively in the figure legend) as a function of ocean depth. The open (i.e. non-solid) shapes correspond to a simulation with doubled ocean width but the full depth, and then the oceanic transport is larger than the atmospheric. (b) Peak transport in the oceanic cold and warm cells as a function of ocean depth. Both plots show the Northern Hemisphere in simulations with no circumpolar channel.

The classical gyre circulation, with a Sverdrup interior and western boundary currents, is completely removed (see lower left panel of Figure 6), and the meridional heat transfer is effected by the deep overturning circulation, Ekman transport and the associated shallow cell at low latitudes and mesoscale eddies, parametrized by a GM scheme in our integration. Because there can be no zonally averaged geostrophic flow in the interior (because the zonally averaged zonal pressure gradient is zero), any net meridional Ekman transport at the surface cannot be returned in the ocean interior (at least by geostrophic flow), and all the transport returns in a bottom boundary layer (see Figure 6); there is no conventional main thermocline and there is no hemispheric-scale meridional overturning circulation. The components of the ocean heat transport (not shown) are, not surprisingly, quite different from the control case. In the control case the mesoscale eddy parametrization makes almost no direct contribution to the energy transport, whereas in the

DOI: 10.1002/qj

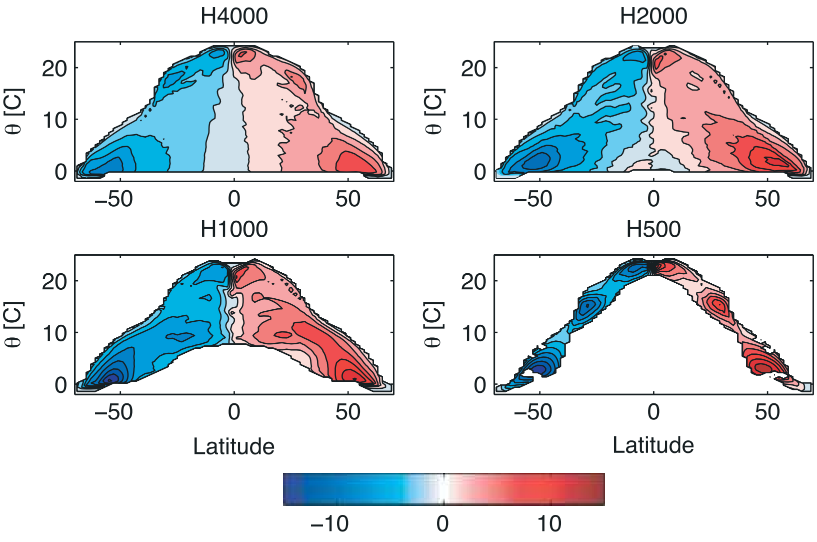

Figure 10. Meridional overturning circulation, with potential temperature as a vertical coordinate, for circulations with varying ocean depths (4000 m, 2000 m etc.). There is no Drake Passage in these simulations.

case with no meridional walls the isopycnals are almost vertical, implying a large store of available potential energy, and the parametrized (GM) contribution is large, as was found by Marshall *et al.* (2007) and Enderton and Marshall (2009).

8. Effects of oceanic diapycnal diffusivity

The value of the diapycnal diffusivity is not well constrained by observations or theory, and it is likely that it varies both spatially and temporally from values of about $1 \times 10^{-5}\mathrm{m}^2\ \mathrm{s}^{-1}$ in the main subtropical thermocline to values possibly hundreds of times as large in the abyss over rough topography and on continental shelves (Ledwell *et al.*, 1993; Gregg, 1998). The average value almost certainly also depends in some way on the mechanical forcing provided by the atmospheric circulation (Munk and Wunsch, 1998), but we regard it as an independent parameter. In our control simulation we use a constant value of $5 \times 10^{-5}\mathrm{m}^2\ \mathrm{s}^{-1}$.

Theory suggests that the mixing-driven component of the oceanic overturning circulation will increase as the half power of the diffusivity, and the heat transport will increase correspondingly if the meridional temperature gradient stays constant. Figure 11 shows the results of experiments in which the diffusivity is changed. Changes in the surface temperature gradient are not large because of the compensation by the atmosphere, and the change in the overturning circulation is roughly as predicted by the theory, although no account is taken of the contribution of the deep wind-driven overturning circulation.

In the Southern Hemisphere, the polewards transport of energy in the ocean also increases with diapycnal diffusivity, and at large values of diffusivity the diffusively controlled component completely dominates the wind-driven component and the circulation becomes close to symmetric across the Equator. The difference between the Northern and Southern Hemisphere oceanic transports stays roughly constant as diffusivity varies, varying between about 0.3 and 0.4 PW, and this is a measure of the northwards energy transport in the wind-driven circulation. (That transport would be about 0.18 PW if the wind-driven circulation were of equal strength in both hemispheres, but it likely weakens in the Northern Hemisphere, an issue we do not explore here.) It is interesting that, in reality and in our control integration, the value of the diapycnal diffusivity is such that the wind-driven and diffusively driven components are of the same order of magnitude, and partially cancel each other in the Southern Hemisphere. One might expect that for sufficiently small values of diffusivity the transport in the Southern Hemisphere would become northwards, but we have not explored this possibility (nor have we seen it in our integrations). The total planetary heat transport stays fairly constant over a range of ocean diffusivities in both Northern and Southern Hemispheres. This result seems consistent with the arguments of Stone (1978), who argued that good compensation would occur if the atmosphere were in a regime with efficient dynamical transport mechanisms.

9. Changing the moisture content of the atmosphere

In this section we examine the effects on the heat transport of variations in the amount of water vapour in the atmosphere. The water vapour content is the product of the relative humidity and the saturation mixing ratio; the latter is determined by the Clausius–Clapeyron relation, which for constant latent heat of vaporization L gives the saturation vapour pressure as a function of temperature,

$$e_s(T) = e_0 \exp\left[-\frac{L}{R}\left(\frac{1}{T} - \frac{1}{T_0}\right)\right], \tag{9.1}$$

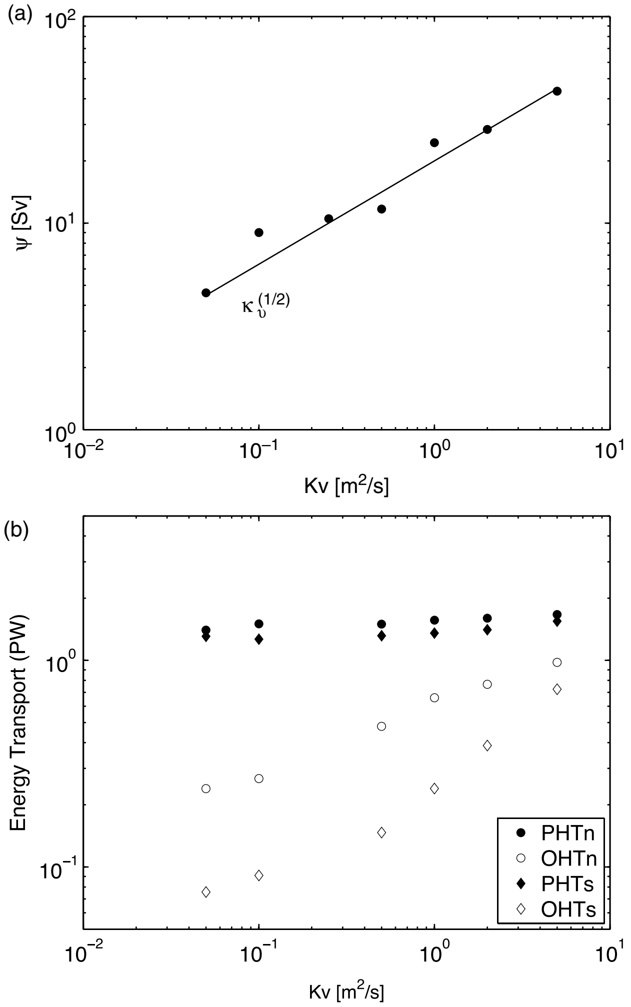

Figure 11. (a) The meridional overturning in the Northern Hemisphere as a function of oceanic diapycnal diffusivity, with a $k_\upsilon^{1/2}$ line drawn. (b) The oceanic heat transport (OHT) and total planetary heat transport (PHT, atmospheric plus oceanic) for both Northern and Southern Hemispheres, in petawatts, as a function of diapycnal diffusivity.

where e_0 is a constant and R is the gas constant. Following Frierson *et al.* (2007), we change the water vapour content of the atmosphere by multiplying e_0 by a constant, $\varepsilon*$, and we have performed integrations with $\varepsilon* = 0.25$, 0.5, 1, 1.5 and 2.0. (Given that saturation vapour pressure increases with temperature by about 7% per degree, the higher values give larger changes in water vapour content than can be expected with global warming.) For each value of $\varepsilon*$ we integrate the coupled model to equilibrium, typically a 1000 year or longer integration, and then take an average over an additional 100 years.

The total energy transport of the atmosphere is the sum of the dry static-energy transport and the latent energy transport, and the midlatitude latent energy transfer increases monotonically with $\varepsilon*$, as seen in the lower right panel of Figure 12. The dry static-energy transfer compensates for the latent energy transport changes; that is to say, the dry static-energy transport tends to fall with increasing moisture, but the compensation is far from perfect and the total atmospheric energy transfer (i.e. the moist static-energy transfer) generally increases as the moisture content of the atmosphere increases, although not in a linear fashion, as shown in the upper right panel of Figure 12 and in Figure 13. Held and Soden (2006) also found compensation between the latent and sensible heat transfer in analysis of global warming simulations with full GCMs, although only in the equilibrium response. This kind of compensation is the opposite of what might be expected during natural variability of the system on decadal time-scales; in that case, the latent energy transfer and the dry static-energy transfer do indeed vary in unison (not shown).

The complicated way the atmosphere responds here is due at least in part to the presence of the ocean: the total oceanic energy transport decreases as the moisture increases (Figure 13), especially at the highest values of moisture content, because of the increased precipitation and concomitant freshening at high latitudes and the associated reduction of the buoyancy-driven overturning circulation. With $\varepsilon* = 2$, the oceanic overturning circulation almost completely shuts off and the oceanic energy transport (Figure 13) drops about a factor of two from its control value, which in turn is more than 50% smaller that its value with $\varepsilon* = 0.25$. The total energy transport of the atmosphere, in turn, does not wholly compensate for the changes in ocean transport, and the net result is that the total meridional energy of the atmosphere and ocean varies by about 20% with variations in $\varepsilon*$, *decreasing* with increased moisture content, with much of that variation occurring at the largest value of $\varepsilon*$ when the energy transport due to the deep overturning circulation of the ocean falls substantially.

10. The distribution of solar radiation

In this section we examine changes in the partitioning of heat transport as the distribution of incoming solar radiation changes. As the Pole–Equator gradient of incoming radiation increases, the atmospheric heat transport will also increase. If the rudimentary scaling arguments of section 4.1 hold, then the surface wind will increase approximately proportionally, and if the ocean gyre heat transport is in a regime where it increases linearly with the wind stress then the atmospheric heat transport and the wind-driven ocean heat transport would similarly increase. However, the energy transport due to the oceanic diffusively driven overturning circulation will not in general change in the same way, increasing fairly slowly with temperature gradient as in (3.6). Let us examine these expectations.

In our model, the incoming solar radiation is given as a function of latitude by

$$S(\vartheta) = \frac{S_0}{4}[1 - \Delta_S P_2(\vartheta)], \qquad (10.1)$$

where S_0 is the solar constant, $P_2(\vartheta)$ is the second Legendre function and Δ_S is a constant. In our control experiment $\Delta_S = 1.2$, and in addition we have conducted integrations with Δ_S ranging from 0.3–1.5. We performed

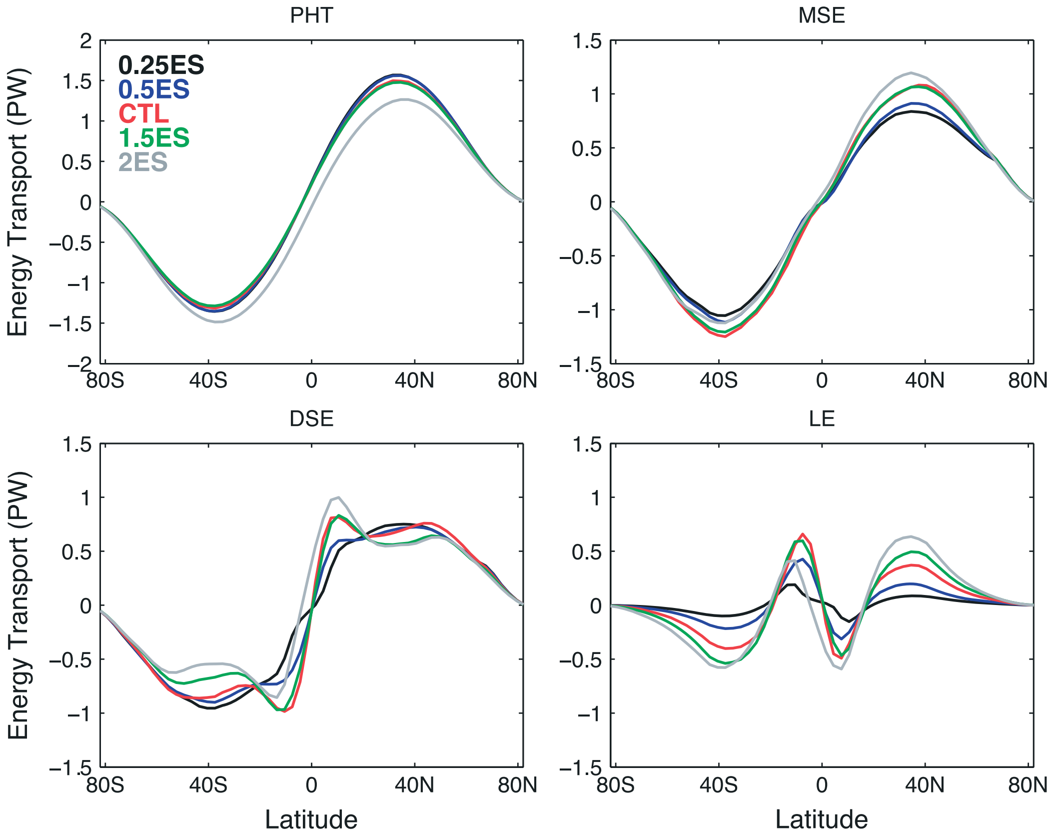

Figure 12. Energy transport on varying the moisture content of the atmosphere. PHT is the planetary (total) transport, MSE is the moist static-energy transport in the atmosphere, DSE is the dry static-energy transfer in the atmosphere and LE is the latent energy transport.

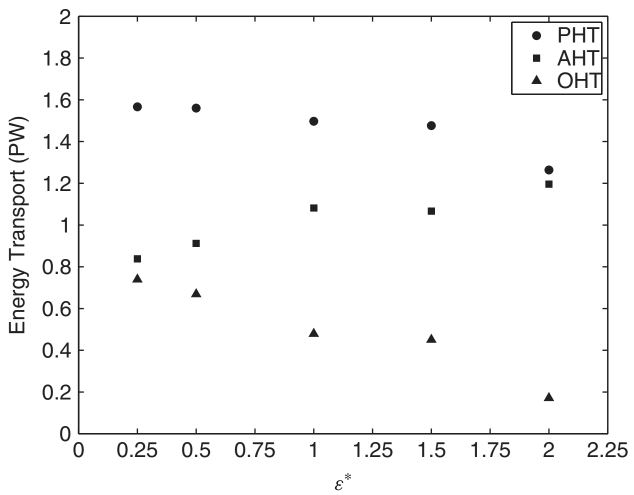

Figure 13. Planetary, atmospheric and oceanic energy transfer in Northern Hemisphere midlatitudes as a function of $\varepsilon*$, the multiplier in Equation (9.1).

this sequence for geometries both with and without a Southern Hemisphere channel; the latter case is symmetric about the Equator and provides a clearer separation of wind-driven and buoyancy-driven circulation. The former case is more realistic, but the lack of such a separation complicates interpretation.

Figure 14 shows the changes in midlatitude atmospheric energy transport and oceanic energy transport, decomposed into the transport of warm cells and cold cells, as Δ_S changes, and Figure 15 shows the distribution with latitude of the oceanic energy transport. The atmospheric energy transport increases with Δ_S (and ΔT, the temperature difference across midlatitudes), and the transport in the warm, largely wind-driven, oceanic cell increases at very nearly the same rate. We do not have a theory for this rate. It is perhaps surprising that the two rates of change are so similar, given the limitations of the scaling arguments of section 5. In the case with a circumpolar channel (not shown), the same qualitative behaviour occurs, but the correspondence between the transport of the atmosphere and ocean gyres is not as close, possibly because warm cells include components driven remotely from the Southern Ocean.

Unlike the gyre transport, the transport of the cold, deep ocean is not proportional to that of the atmosphere, increasing more slowly with Δ_S. (Note also that the deep transport can be expected to respond primarily to the temperature difference across the subpolar gyre (Samelson and Vallis, 1997).) At sufficiently large values of Δ_S we expect that the transport in the wind-driven warm cells will exceed that of the cold cells, although we have not attempted to reach that limit. The picture of the overturning circulation of the ocean reflects these results, as shown in Figure 16; the warm cells stand out much more clearly as the meridional gradient increases, and for small values of Δ_S the warm cells are almost non-existent.

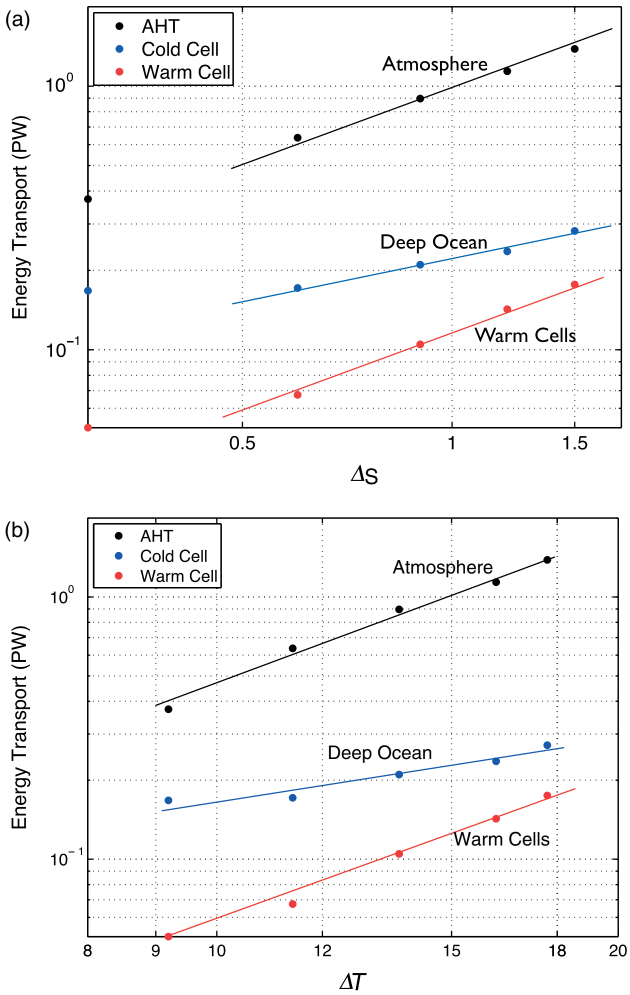

Figure 14. (a) Midlatitude Northern Hemisphere atmospheric and oceanic heat transport, in petawatts, as a function of Δ_S, with the oceanic transport decomposed into that due to deep cold cells and warm, wind-driven cells, in a sequence of simulations with no circumpolar channels. (b) Same results, now plotted against the surface temperature difference from 30°N and 60°N. The upper (black) and lower (red) solid lines are parallel to each other in each panel.

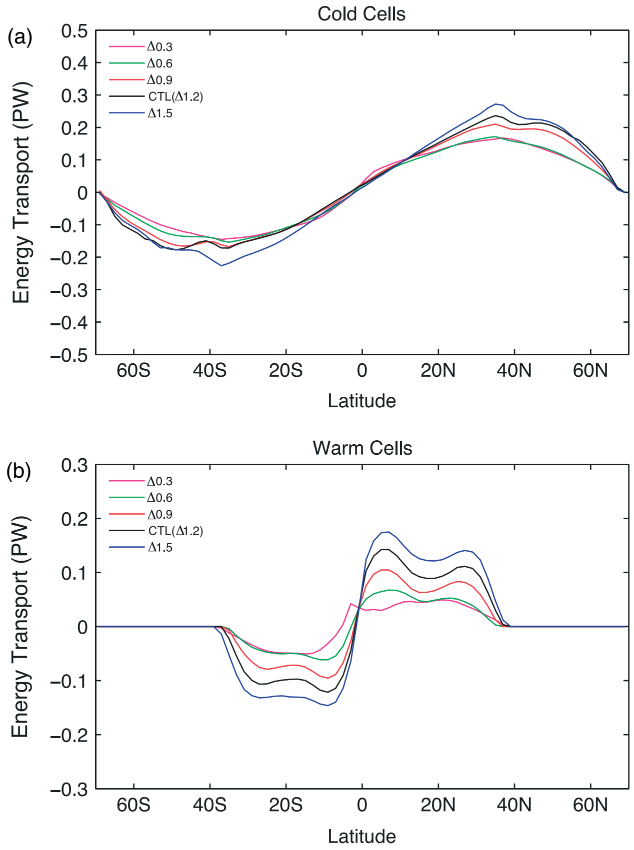

Figure 15. Oceanic energy transport for (a) cold cells and (b) warm cells for various values of Δ_S (from 0.3–1.5), for simulations with no circumpolar channel.

11. Changing the rotation rate

As in the case of variations in the meridional distribution of solar radiation, there is little quantitative theory to guide us regarding how the magnitude of the atmospheric energy transport will respond to changes in the rotation rate, Ω, although a number of simulations have been carried out, some in the context of planetary atmospheres (Hunt, 1979; Del Genio and Zhou, 1996; Barry *et al.*, 2002; Williams, 2003; Schneider and Walker, 2008; Zurita-Gotor and Vallis, 2009). Our heuristic expectations are that the meridional transport in midlatitudes will generally decrease with increasing Ω because, as noted by Hunt, increasing the rotation rate will tend to diminish the scale of flow structures, reducing the efficiency of the meridional energy transport. The flow will also become increasingly zonal as β increases, inhibiting meridional transport. Reducing the rotation rate may also allow the Hadley cell to expand, potentially leading to enhanced low-latitude meridional heat transport. The mean surface wind will not necessarily correspondingly diminish with increased rotation, because it is the β-effect that produces Rossby waves that leads to a convergence of eddy momentum flux balanced by surface drag. In spite of all this uncertainty, the scaling of section 5 suggests that the heat transport of the warm oceanic cells will vary with the rotation rate in very roughly the same way as that of the atmosphere, if the atmosphere does not enter a different dynamical regime or significantly change its moisture content.

The overall effects of changing the rotation rate on the meridional energy transfer are illustrated in Figure 17. (At high rotation rates the atmospheric flow structures are smaller and so we also performed experiments at more than double the resolution, 1.5° × 1.5°, in the atmospheric model. The high-resolution results show small quantitative differences from the lower resolution runs at the highest rotation rates, but confirm the general results.) The total meridional energy transfer of the coupled system decreases by about a factor of three as the rotation rate increases over the range shown. The oceanic heat transport in the deep cells (the MOC) does not diminish as rapidly, and for the largest values of rotation the oceanic heat transfer is larger than that of the atmosphere. For small rotation rates the atmospheric heat transport is roughly constant, although the limited longitudinal extent of the model may constrain the size of the eddies and affect the heat transport.

DOI: 10.1002/qj

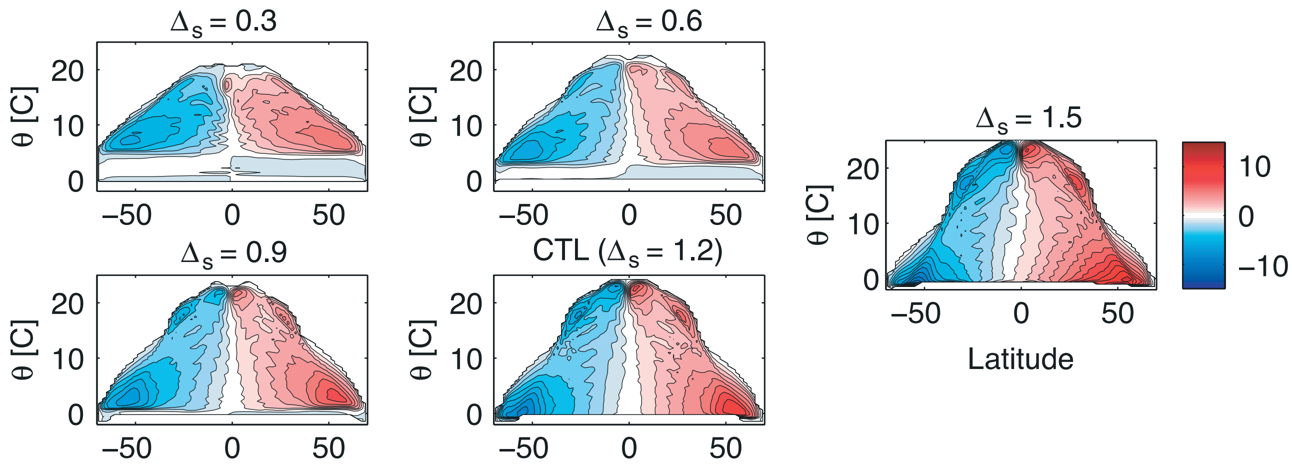

Figure 16. The stream function, in potential temperature space, as Δ_S changes, for an inter-hemispherically symmetric (no ACC) configuration. Increased values correspond to a larger gradient of incoming solar radiation between Equator and Pole, and a value of 1.2 corresponds to the control simulation. The intensity of the wind-driven cells increases faster with Δ_S than does that of the deep cell.

The decomposition of the oceanic heat transport into cold cells and warm cells is shown in Figure 17. Although none of the transports in the figure evinces a clean scaling law, two features are apparent.

(1) The energy transport of the cold oceanic cell varies rather weakly with rotation rate, as might be expected from Equation (3.6).
(2) The atmospheric energy transport falls quite rapidly at high values of rotation rate (compared with the energy transfer in the deep ocean), consistent with the results of many previous atmosphere-only simulations. The wind-driven transport in the ocean qualitatively tracks the atmospheric transport, although it falls faster than that of the atmosphere at high rotation rates, suggesting that the gyral transport is becoming relatively inefficient and may be entering the regime in which the heat transport varies quadratically with wind-stress, as discussed by Wang *et al.* (1995) and in section 3.1. As the rotation rate is lowered from its current value, the atmospheric heat transport does not keep on increasing and the oceanic heat transport of the gyres increases only slowly.

12. Discussion and conclusions

In this article we have been concerned with the mechanisms of meridional energy transport in the coupled atmosphere–ocean system, focusing on mid and high latitudes. Here, the atmospheric energy transport is effected by baroclinic eddies, and oceanic energy transport in mid-latitudes is effected by both wind-driven gyres and the deep meridional overturning circulation. We have used a simply configured coupled atmosphere–ocean model in conjunction with simple scaling arguments to try to understand the partitioning of the transport between atmosphere and ocean.

The observed and modelled ocean heat transport, (Figure 4) is a maximum close to the Equator and then falls almost monotonically polewards. The atmospheric heat transport rises more slowly from close to zero at the Equator to a maximum at about 40°N before falling to zero again at the Poles. For Earth-like parameters our model atmosphere transports over twice as much energy polewards as the ocean over much of the midlatitudes, but this ratio is not fixed. The oceanic energy transport may be increased by increasing the width of the ocean and/or its diapycnal diffusivity, or by reducing the effective moisture content of the atmosphere: less moisture and less precipitation at high latitudes serves to increase the meridional buoyancy gradient at the surface and thus the strength of the MOC. If we double the width of our model ocean (so that it has the same zonal extent as our atmosphere), it transports more energy polewards than our model atmosphere. There is evidently no a priori reason why the ocean cannot transport more energy than the atmosphere, but for Earth-like parameters this is not the case.

The energy transport by the ocean is less in the Southern Hemisphere than in the Northern, both in our simulations and in reality. In our model, and possibly in reality, this is due to a partial cancellation between the diffusively driven circulation, which transports energy polewards, and the wind-driven overturning circulation, which transports energy northwards, and so equatorwards, in the Southern Hemisphere. The wind-driven overturning circulation enhances the northwards energy transport in the Northern Hemisphere, and so if the circumpolar channel is blocked then the polewards energy transport in the Southern Hemisphere is increased, but that in the Northern Hemisphere is diminished. If the ocean's diapycnal diffusivity is increased, then the polewards energy transport increases in both hemispheres. On Earth, these effects occur primarily in the Atlantic, where the overturning circulation in fact transports heat northwards in both hemispheres.

The ocean's energy transport in classical wind-driven gyres is, by definition, a consequence of the surface stress, and rudimentary scaling arguments suggest that

DOI: 10.1002/qj

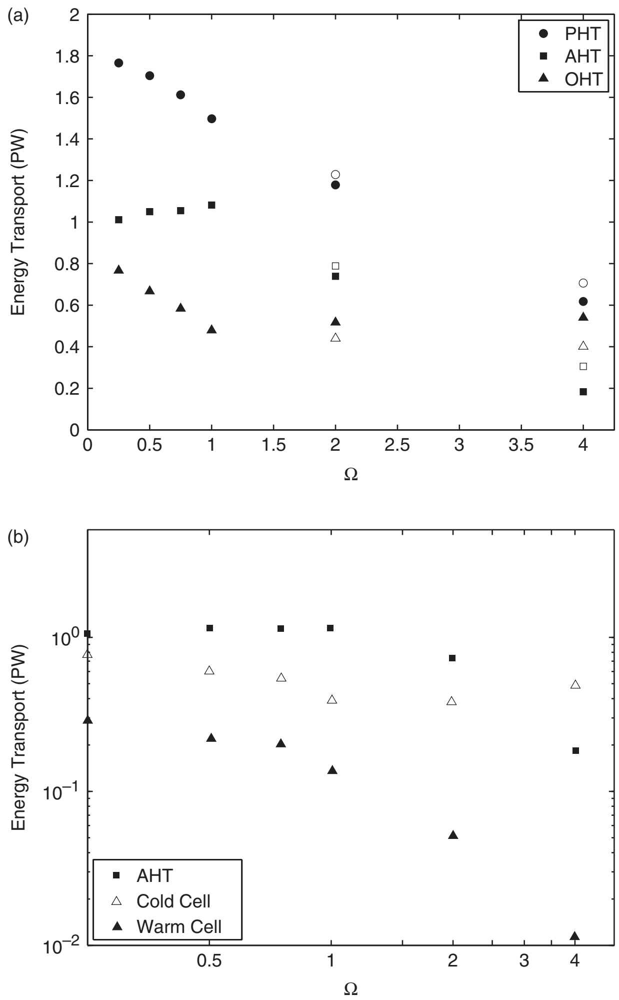

Figure 17. (a) The midlatitude energy transfer of the atmosphere (AHT), ocean (OHT) and their sum (PHT) as a function of rotation rate (normalized by the present-day value), on a linear scale. The values are averages from 20°–60°N. The open symbols denote corresponding simulations with higher resolution in the atmospheric model. (b) Energy transfer in the atmosphere, ocean cold cell and ocean warm cell as a function of rotation rate, on a log – log scale.

the energy transport in the ocean's wind-driven ocean gyres will vary in a roughly similar fashion to the energy transport of the atmosphere as external parameters vary, provided the atmosphere does not move into a different regime. This expectation is met in the case in which the meridional gradient of incoming solar forcing is varied (see Figure 14), although it is only qualitatively supported as the rotation rate is varied. Changing the rotation rate undoubtedly has effects on the dynamics of both atmosphere and ocean beyond those considered here. Nevertheless, the transport of the ocean's wind-driven gyres does vary with rotation in a more similar fashion to the atmosphere than does the transport of the deep ocean circulation (Figure 17).

If the moisture in the atmosphere is increased, by changing a parameter in the idealized Clausius – Clapeyron relation, then the atmospheric energy transport generally increases, especially in midlatitudes, because of an increase in the latent heat transfer, even though the dry static-energy transfer diminishes. However, the overall ocean transport diminishes, primarily because of a decreased surface buoyancy gradient, associated with increased precipitation at high latitudes, that serves to diminish the deep overturning cell. This effect is monotonic, and at very high moisture levels the overturning circulation of the ocean switches off almost entirely. The net effect is that the total (atmospheric plus oceanic) meridional energy transport *diminishes* with increasing moisture content, most noticeably at the highest values of moisture. The relevance of this to global warming, if any, is hard to gauge, for the shut-off in the ocean's deep overturning circulation occurs when the moisture content is about double the present amount, which is a very large change unlikely to occur naturally. For smaller changes in moisture, the changes in total energy transport are much smaller.

If the oceanic parameters (e.g. its diapycnal diffusivity) are changed, thus changing the ocean's energy transport, then we find that over a fairly wide range of parameters the atmosphere is able to compensate fairly well, and the total meridional transport remains fairly constant. We attribute this to the efficiency of the atmosphere in responding to changes in temperature gradients. At low latitudes the compensation is not as good, because a greater proportion of the ocean's energy transport is a direct response to the wind forcing from the atmosphere. In general the total meridional energy transport of the atmosphere plus ocean is not fixed, and is *not* just a function of incoming solar radiation and albedo. Rather, it varies to a greater or lesser degree with rotation rate, moisture content, geometry and ocean mixing, and there is no a priori requirement that the latitudinal distribution top-of-the-atmosphere radiation balance remains the same. Notably, we find that the total energy transport in the coupled system diminishes as the planetary rotation rate increases and the atmosphere enters a regime in which meridional energy transfer is relatively inefficient. Good compensation by the atmosphere does occur when one changes some oceanic parameter, such as diapycnal diffusivity, if the atmosphere is in a regime of efficient energy transport.

To conclude, in this article we provided only a rudimentary overall view of the main mechanisms determining the partitioning and magnitude of energy transport in the atmosphere–ocean system; we hope that future work may build on this.

Acknowledgements

We thank an anonymous reviewer for very useful and constructive criticism. The work was funded by the NSF and by NOAA.

References

Barry L, Craig GC, Thuburn J. 2002. Poleward heat transport by the atmospheric heat engine. *Nature* **415**: 774–777.

Bryan K, Sarmiento JL. 1985. Modeling ocean circulation. *Adv. Geophys.* **28**: 433–459.

DOI: 10.1002/qj

Bye J, Veronis G. 1980. Poleward heat flux by an ocean gyre. *Dyn. Atmos. Oceans* **4**: 101–114.

Caballero R, Langen PL. 2005. The dynamic range of poleward energy transport in an atmospheric general circulation model. *Geophys. Res. Lett.* **32**: L02 705. DOI: 10.1029/2004GL021581.

Cessi P. 2000. Thermal feedback on wind stress as a contributing cause of climate variability. *J. Climate* **13**: 232–244.

Czaja A, Marshall J. 2006. The partitioning of poleward heat transport between the atmosphere and ocean. *J. Atmos. Sci.* **63**: 1498–1511.

Del Genio A, Zhou W. 1996. Simulations of superrotation on slowly rotating planets: Sensitivity to rotation and initial condition. *Icarus* **120**: 332–343.

Eady ET. 1957. 'The general circulation of the atmosphere and oceans'. In *The Earth and its Atmosphere*, Bates DR (ed). Basic Books: New York; pp. 130–151.

Enderton D, Marshall J. 2009. Explorations of atmosphere–ocean–ice climates on an aquaplanet and their meridional energy transports. *J. Atmos. Sci.* **66**: 1593–1611.

Farneti R, Vallis GK. 2009. An intermediate complexity climate model (ICCM) based on the GFDL flexible modelling system. *Geosci. Model Dev.* **2**: 73–81. http://www.geosci-model-dev-discuss.net/2/341/2009/.

Frierson DMW, Held IM, Zurita-Gotor P. 2006. A gray radiation aquaplanet moist GCM. Part 1: Static stability and eddy scales. *J. Atmos. Sci.* **63**: 2548–2566.

Frierson DMW, Held IM, Zurita-Gotor P. 2007. A gray radiation aquaplanet moist GCM. Part 2: Energy transports in altered climates. *J. Atmos. Sci.* **64**: 1680–1693.

Gallego B, Cessi P. 2000. Exchange of heat and momentum between the atmosphere and the ocean: a minimal model of decadal oscillations. *Clim. Dyn.* **16**: 479–489.

Ganachaud A, Wunsch C. 2000. Improved estimates of global ocean circulation heat transport and mixing from hydrographic data. *Nature* **408**: 453–457.

Gent PR, McWilliams JC. 1990. Isopycnal mixing in ocean circulation models. *J. Phys. Oceanogr.* **20**: 150–155.

Gnanadesikan A. 1999. A simple predictive model for the structure of the oceanic pycnocline. *Science* **283**: 2077–2099.

Green JSA. 1970. Transfer properties of the large-scale eddies and the general circulation of the atmosphere. *Q. J. R. Meteorol. Soc.* **96**: 157–185.

Gregg MC. 1998. 'Estimation and geography of diapycnal mixing in the stratified ocean'. In *Physical Processes in Lakes and Oceans*, Imberger J (ed). American Geophysical Union; pp. 305–338.

Gutowski WJ. 1985. Baroclinic adjustment and midlatitude temperature profiles. *J. Atmos. Sci.* **42**: 1733–1745.

Gutowski WJ, Branscome LE, Stewart DA. 1989. Mean flow adjustment during lifecycles of baroclinic waves. *J. Atmos. Sci.* **46**: 1724–1737.

Held IM. 2001. The partitioning of the poleward energy transport between the tropical ocean and atmosphere. *J. Atmos. Sci.* **58**: 943–948.

Held IM, Larichev VD. 1996. A scaling theory for horizontally homogeneous, baroclinically unstable flow on a beta-plane. *J. Atmos. Sci.* **53**: 946–952.

Held I, Soden B. 2006. Robust responses of the hydrological cycle to global warming. *J. Climate* **19**: 5686–5699.

Hunt BG. 1979. The influence of the Earth's rotation rate on the general circulation of the atmosphere. *J. Atmos. Sci.* **36**: 1392–1407.

Ledwell JR, Watson AJ, Law CS. 1993. Evidence for slow mixing across the pycnocline from an open-ocean tracer-release experiment. *Nature* **363**: 701–703.

Leovy C. 1973. Exchange of water vapor between the atmosphere and surface of Mars. *Icarus* **18**: 120–125.

Marshall J, Ferreira D, Campin JM, Enderton D. 2007. Mean climate and variability of the atmosphere and ocean on an aquaplanet. *J. Atmos. Sci.* **64**: 4270–4286.

Munk WH, Wunsch C. 1998. Abyssal recipes II: energetics of tidal and wind mixing. *Deep-Sea Res.* **45**: 1976–2009.

Neelin JD, Held I. 1987. Modeling tropical convergence based on the moist static energy budget. *Mon. Weather Rev.* **115**: 3–12.

O'Gorman PA, Schneider T. 2006. Stochastic models for the kinematics of moisture transport and condensation in homogeneous turbulent flows. *J. Atmos. Sci.* **63**: 2992–3005.

O'Gorman PA, Schneider T. 2008. The hydrological cycle over a wide range of climates simulated with an idealized gcm. *J. Climate* **21**: 3815–3832.

Pedlosky J. 1996. *Ocean circulation theory*. Springer-Verlag: Berlin.

Pierrehumbert RT, Brogniez H, Roca R. 2006. 'On the relative humidity of the atmosphere'. In *The Global Circulation of the Atmosphere: Phenomena, Theory, Challenges*, Schneider T, Sobel A (eds). Princeton University Press: Princeton; pp. 143–185.

Robinson AR, Stommel H. 1959. The oceanic thermocline and the associated thermohaline circulation. *Tellus* **11**: 295–308.

Samelson RM. 2004. Simple mechanistic models of middepth meridional overturning. *J. Phys. Oceanogr.* **34**: 2096–2103.

Samelson RM, Vallis GK. 1997. Large-scale circulation with small diapycnal diffusion: the two-thermocline limit. *J. Mar. Res.* **55**: 223–275.

Schneider T, Walker CC. 2008. Scaling laws and regime transitions of macroturbulence in dry atmospheres. *J. Atmos. Sci.* **65**: 2153–2173.

Sijp WP, England MH. 2004. Effect of the Drake Passage throughflow on global climate. *J. Phys. Oceanogr.* **34**: 1254–1266.

Stone PH. 1978. Constraints on dynamical transport of energy on a spherical planet. *Dyn. Atmos. Oceans* **2**: 123–139.

Stone PH, Yau MS. 1990. Development of a two-dimensional zonally averaged statistical-dynamical model. Part III: the parameterization of the eddy fluxes of heat and moisture. *J. Climate* **3**: 726–740.

Toggweiler JR, Samuels B. 1998. On the ocean's large-scale circulation in the limit of no vertical mixing. *J. Phys. Oceanogr.* **28**: 1832–1852.

Trenberth KE, Caron JM. 2001. Estimates of meridional atmosphere and ocean heat transports. *J. Climate* **14**: 3433–3443.

Vallis GK. 1982. A statistical dynamical climate model with a simple hydrology cycle. *Tellus* **34**: 211–227.

Vallis GK. 2000. Large-scale circulation and production of stratification: effects of wind, geometry and diffusion. *J. Phys. Oceanogr.* **30**: 933–954.

Vallis GK. 2006. *Atmospheric and oceanic fluid dynamics*. Cambridge University Press: Cambridge, UK.

Wang X, Stone PH, Marotzke J. 1995. Poleward heat transport in a barotropic ocean model. *J. Phys. Oceanogr.* **25**: 256–265.

Warren BA. 1999. Approximating the energy transport across oceanic sections. *J. Geophys. Res.* **104**: 7915–7920.

Welander P. 1986. 'Thermohaline effects in the ocean circulation and related simple models'. In *Large-scale Transport Processes in Oceans and Atmospheres*, Willebrand J, Anderson DLT (eds). Reidel: Dordrecht; pp. 163–200.

White AA, Green JSA. 1984. Transfer coefficient eddy flux parameterizations in a simple model of the zonal average atmospheric circulation. *Q. J. R. Meteorol. Soc.* **110**: 1035–1052.

Williams GP. 2003. Barotropic instability and equatorial superrotation. *J. Atmos. Sci.* **60**: 2136–2152.

Zurita-Gotor P, Vallis GK. 2009. Equilibration of baroclinic turbulence in primitive equations and quasi-geostrophic models. *J. Atmos. Sci.* **66**: 837–863.